Dual-algorithm wavefield extrapolation applied to depth imaging

Yanpeng Mi and Gary F. Margrave

ABSTRACT

The dual-extrapolation algorithm using large-step nonstationary wavefield extrapolators and vertical wavefield interpolation for depth imaging is reviewed. The PSPI dual-algorithm is applied to complex-structure prestack depth imaging from both flat and topographic recording surfaces. The imaging results are compared with images produced by other authors using different algorithms. It is shown that the dual-algorithm is capable of imaging very complicated structures.

INTRODUCTION

Complex geology requires increasing the number of reference velocities in Gazdag's PSPI (Gazdag and Sguazzero, 1984) and the number of spatial windows for the windowed split-step Fourier algorithm, which significantly increases the amount of computing time. The recursive nonstationary integral algorithms (PSPI, NSPS and SNPS) are accurate however too slow for many purposes. With small vertical and lateral velocity gradients, large extrapolation steps can be taken without causing noticeable errors. Ng (1994) demonstrated that large time steps could be used in Gazdag's PSPI; however he did not recognize that different velocities should be used for the static phase-shift and the focusing phase-shift. The dual extrapolation algorithm (Mi and Margrave, 2000) splits the total phase-shift in complex media into a static phase-shift, which is computed with the time-average velocity in the (ω, x) domain, and a focusing phase-shift, which is computed with the depth-average velocity using the nonstationary integrals. High accuracy is achieved when the extrapolation step is not too large and the velocity gradients are reasonably small. This significantly reduces the run time of the recursive integral wavefield extrapolators. The dual algorithm can be conveniently applied to the flat datum imaging problem and extended to the topographic imaging problem with minor modifications to the theory.

THE DUAL-EXTRAPOLATION ALGORITHM FOR PRESTACK DEPTH IMAGING

In media of constant velocity, considering downward extrapolation only, the phase-shift that carries the wavefield from 0 to z can be split into a static phase shift in the (ω, x) domain and a focusing phase-shift in the (ω, k_x) domain

$$\begin{aligned}
\Phi &= z\sqrt{\frac{\omega^2}{v^2} - k_x^2} = \Phi_{static} + \Phi_{focus} \\
\Phi_{static} &= \frac{\omega z}{v} \\
\Phi_{focus} &= \frac{\omega z}{v}\left(\sqrt{1 - \frac{k_x^2 v^2}{\omega^2}} - 1\right),
\end{aligned} \tag{1}$$

where Φ_{static} is applied in the (ω, x) domain, and the focusing term Φ_{focus} is applied in the (ω, k_x) domain.

Equation (1) is exact for homogeneous media. It is also approximately applicable for $v(z)$ media by replacing the focusing velocity with a root-mean-square (RMS) velocity. Applied recursively, this is equivalent to a WKBJ solution to the scalar wave equation. Equation (1) can be generalized to media with weak lateral-velocity variation. Both the static and the focusing phase-shift become functions of spatial location x

$$\begin{aligned}
\Phi(x) &= z\sqrt{\frac{\omega^2}{v^2(x)} - k_x^2} = \Phi(x)_{static} + \Phi(x)_{focus} \\
\Phi(x)_{static} &= \frac{\omega z}{v(x)} \\
\Phi(x)_{focus} &= \frac{\omega z}{v(x)}\left(\sqrt{1 - \frac{k_x^2 v(x)^2}{\omega^2}} - 1\right)
\end{aligned} \quad . \tag{2}$$

Similar to the case of constant velocity, the static phase-shift $\Phi(x)_{static}$ is applied in (ω, x) domain, which corresponds to a spatially varying vertical traveltime. The focusing phase-shift $\Phi(x)_{focus}$ is applied as a nonstationary filter in (ω, k_x) domain, which corresponds to the energy propagating in all possible angles.

Substitution of equation (1) into the nonstationary wavefield extrapolator gives a split nonstationary operator

$$\alpha(\mathrm{x}, \mathrm{k}_\mathrm{x}, z, \omega) = e^{-i(\Phi(x)_{static} + \Phi(x)_{focus})} \quad . \tag{3}$$

The PSPI and NSPS integral extrapolation can then be written as

$$\psi_{PSPI}(\mathrm{x}, z, \omega) = e^{-i\Phi(x)_{static}}\left[\frac{1}{(2\pi)^2}\int_{-\infty}^{+\infty}\alpha'(\mathrm{x}, \mathrm{k}_\mathrm{x}, z, \omega)\varphi(\mathrm{k}_\mathrm{x}, 0, \omega)\exp(-i\mathrm{k}_\mathrm{x}x)d\mathrm{k}_\mathrm{x}\right] \tag{4}$$

and

$$\varphi_{NSPS}(\mathrm{k_x},z,\omega)=\int_{-\infty}^{+\infty}\alpha'(\mathrm{x},\mathrm{k_x},z,\omega)\left[\psi(\mathrm{x},0,\omega)e^{-i\Phi(x)_{static}}\right]\exp(i\mathrm{k_x}x)d\mathrm{x}\quad, \tag{5}$$

respectively. $\alpha'(\mathrm{x},\mathrm{k_x},z,\omega)$ is now the nonstationary focusing operator

$$\alpha'(\mathrm{x},\mathrm{k_x},z,\omega)=e^{-i\frac{\omega z}{v(x)}\left(\sqrt{1-\frac{k_x^2v(x)^2}{\omega^2}}-1\right)}\quad. \tag{6}$$

Equations (4) and (5) can be written in the form of a matrix-vector multiplication with the (ω,x) domain static phase shift term applied before (for NSPS) and after (for PSPI) application of the nonstationary focusing term.

For $v(z)$ media, both the static and focusing phase-shift become independent of x and they can be accumulated over depth. The accumulated static phase-shift can be written as

$$\Phi_{static}=\int_0^z\frac{\omega}{v(z')}dz'=\frac{\omega z}{v_{ave}(z)}\quad. \tag{7}$$

The accumulated focusing term can be written as

$$\Phi_{focus}=\int_0^z\frac{\omega}{v(z')}\left(\sqrt{1-\frac{k_x^2v(z')^2}{\omega^2}}-1\right)dz'\quad. \tag{8}$$

Equation (7) together with (8) gives a WKBJ solution for *v(z)* media. For media with lateral-velocity variation, equation (7) remains valid, however equation (8) does not since the PSPI and NSPS integrals don't perform exact inverse- or forward-spatial Fourier transforms. PSPI and NSPS thus become local integral operators that don't directly accumulate over depth. However, for weak lateral velocity variation, the focusing term approximately accumulates and equation (8) can be generalized to

$$\Phi_{focus}=\int_0^z\frac{\omega}{v(x,z')}\left(\sqrt{1-\frac{k_x^2v(x,z')^2}{\omega^2}}-1\right)dz'\quad. \tag{9}$$

The static phase-shift still accumulates exactly

$$\Phi_{static}=\int_0^z\frac{\omega}{v(x,z')}dz'=\frac{\omega z}{v_{ave}(x,z)}\quad. \tag{10}$$

Expanding the square-root term in equation (9) with binomial expansion leads to,

$$\Phi_{focus} = -\frac{k_x^2 z}{2\omega}\frac{1}{z}\int_0^z v(x,z')dz' - \frac{k_x^4 z}{8\omega^3}\frac{1}{z}\int_0^z v(x,z')^3 dz' + \frac{k_x^6}{16\omega^5}\frac{1}{z}\int_0^z v(x,z')^5 dz' - \ldots \quad (11)$$

Note the $\frac{1}{z}\int_0^z v(x,z')dz'$ is exactly the depth-average velocity (mean velocity) defined as

$$v_{mean} = \frac{1}{z}\int_0^z v(z')dz' \quad . \quad (12)$$

This suggests that the equation (11) can be approximated by

$$\Phi'_{focus} = \frac{\omega z}{v_{mean}(x,z)}\left(\sqrt{1-\frac{k_x^2 v_{mean}(x,z)^2}{\omega^2}} - 1\right). \quad (13)$$

Expanding the equation (13) with power series and then subtracting equation (11) leads to the error term of the focusing phase-shift

$$\Phi_{error} = \frac{k_x^4 z}{8\omega^3}\left(\frac{1}{z}\int_0^z v(x,z')^3 dz' - v_{mean}(x,z)^3\right) + \frac{k_x^6 z}{16\omega^5}\left(\frac{1}{z}\int_0^z v(x,z')^5 dz' - v_{mean}(x,z)^5\right) + \ldots \quad . \quad (14)$$

This error can generally be ignored when 1) propagation angle is small or 2) the depth step z is small or 3) the lateral velocity gradient is small.

For large-step extrapolation, equations (4) and (5) become

$$\psi(\mathrm{x}, z, \omega) = e^{-i\frac{\omega z}{v_{ave}(x)}}\left[\frac{1}{(2\pi)^2}\int_{-\infty}^{+\infty}\alpha'_{mean}(\mathrm{x},\mathrm{k_x},z,\omega)\varphi(\mathrm{k_x},0,\omega)\exp(-i\mathrm{k_x}x)d\mathrm{k_x}\right] \quad (15)$$

and

$$\varphi(\mathrm{k_x}, z, \omega) = \int_{-\infty}^{+\infty}\alpha'_{mean}(\mathrm{x},\mathrm{k_x},z,\omega)\left[\psi(\mathrm{x},0,\omega)e^{-i\frac{\omega z}{v_{ave}(x)}}\right]\exp(i\mathrm{k_x}x)d\mathrm{x} \quad , \quad (16)$$

where $\alpha'_{mean}(\mathrm{x},\mathrm{k_x},z,\omega)$ is now the mean nonstationary focusing operator

$$\alpha'_{mean}(\mathrm{x},\mathrm{k_x},z,\omega) = e^{-i\frac{\omega z}{v_{mean}(x)}\left(\sqrt{1-\frac{k_x^2 v_{mean}(x)^2}{\omega^2}}-1\right)} \quad . \quad (17)$$

Similar to the natural combination of the recursive NSPS and PSPI (Ferguson and Margrave, 1999b), equations (15) and (16) can also be combined naturally to form a symmetric wavefield extrapolator. The symmetric large-step extrapolation from depth 0 to z can be easily formulated as

$$\psi(\mathrm{x},z,\omega)=e^{-i\frac{\omega z}{2v_{ave(z/2\to z)}(x)}}\left[\frac{1}{(2\pi)^2}\int_{-\infty}^{+\infty}\alpha'_{mean(z/2\to z)}(\mathrm{x},\mathrm{k_x},z,\omega)\varphi(\mathrm{k_x},z/2,\omega)\exp(-i\mathrm{k_x}x)d\mathrm{k_x}\right], \quad (18)$$

where

$$\varphi(\mathrm{k_x},z/2,\omega)=\int_{-\infty}^{+\infty}\alpha'_{mean(0\to z/2)}(\mathrm{x},\mathrm{k_x},z/2,\omega)\left[\psi(\mathrm{x},0,\omega)e^{-i\frac{\omega z}{2v_{ave(0\to z/2)}(x)}}\right]\exp(i\mathrm{k_x}x)d\mathrm{x}, \quad (19)$$

and symbols $(0\to z/2)$ and $(z/2\to z)$ denote the depth interval from 0 to z/2 and z/2 to z.

Equations (15) and (16) require the same amount of computation effort as the recursive PSPI and NSPS integral as described before; however, they allow a larger extrapolation step. The maximum allowable depth-step under the condition of limited phase-error is dependent on the complexity of the velocity field and the maximum angle to be imaged.

The large-step extrapolation algorithm can be used to compute the reference wavefields at a depth grid coarser than the imaging depth grid. A linear interpolation between these reference wavefields, after proper vertical traveltime correction, can then be used for produce intermediate wavefields to produce the depth image. The intermediate wavefields are correct in terms of vertical traveltime; however, are slightly mis-focused. Figure 1 shows a schematic drawing of the dual algorithm.

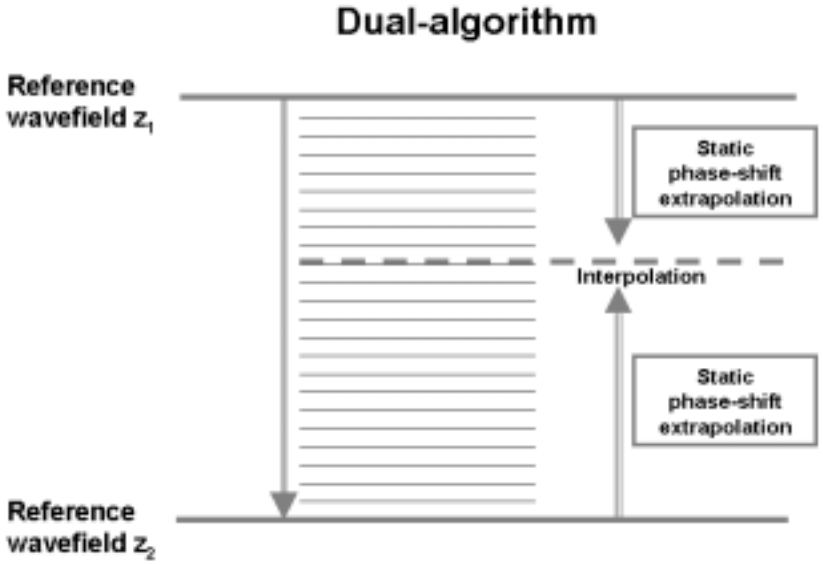

FIG. 1. The dual algorithm uses a accurate algorithm to produce and relatively accurate reference wavefields at a depth grid coarser than the imaging depth grid. Intermediate wavefields can then be computed by fast interpolation.

Consider two (ω, x) domain mono-frequency reference wavefields at z_1 and z_2, $\psi(\mathrm{x}, z_1, \omega)$, $\psi(\mathrm{x}, z_2, \omega)$, which are computed by the large-step PSPI integral extrapolator. An intermediate wavefield between z1 and z2, $\psi(\mathrm{x}, z, \omega)$, can be computed by either forward extrapolation from the wavefield at z_1 or by inverse extrapolation from the wavefield at z_2. However, computation of the focusing term with laterally varying velocity is time-consuming. Since the velocity variation and distance between the upper and lower reference wavefields are small, the upper reference wavefield becomes an under-focused version of the intermediate wavefield and the lower reference wavefield becomes an over-focused version of the intermediate wavefield after vertical traveltime correction. The error in focusing terms can roughly cancel if appropriate weighting factors are applied.

Vertical traveltime correction to the upper and lower reference wavefields produces two approximations to the intermediate wavefield $\psi(\mathrm{x}, z, \omega)$. They can be written as

$$\psi_1'(\mathrm{x}, z, \omega) = \psi(\mathrm{x}, z_1, \omega) e^{-\frac{i(z-z_1)\omega}{v_{ave1}(x)}} \tag{20}$$

and

$$\psi_2'(\mathrm{x}, z, \omega) = \psi(\mathrm{x}, z_2, \omega) e^{\frac{i(z-z_2)\omega}{v_{ave2}(x)}}, \tag{21}$$

where v_{ave1} and v_{ave2} are average velocities from z_1 to z and z to z_2.

Equations (20) and (21) are vertical time corrections. Another slightly slower approach is to use single-reference-velocity split-step Fourier algorithm to approximately correct for the focusing error.

Wavefield weighting can be done by linear interpolation between $\psi_1'(\mathrm{x}, z, \omega)$ and $\psi_2'(\mathrm{x}, z, \omega)$ roughly cancels the focusing error if the difference between v_{ave1} and v_{ave2} is small

$$\psi(\mathrm{x}, z, \omega) \approx \frac{z_2 - z}{z_2 - z_1} \psi_1'(\mathrm{x}, z, \omega) + \frac{z - z_1}{z_2 - z_1} \psi_2'(\mathrm{x}, z, \omega). \tag{22}$$

For a larger difference between v_{ave1} and v_{ave2}, correction for the focusing term is required. A single-reference- velocity split-step Fourier algorithm improves the high-dipping-angle events without slowing down the dual algorithm much.

APPLICATION TO THE MARMOUSI SYNTHETIC DATA

Figure 2 show two imaging tests with a 40m dual PSPI algorithm. Each large-step includes 10 imaging steps at 4m interval. Both vertical static-phase-shift and the single-reference-velocity split-step phase corrections are tested and the results are shown in Figure 2a and Figure 2b. As a result of the focusing phase error introduced

by the vertical traveltime correction, the events on the middle left of the image of **Figure 2a**, as marked with 'poor image', are discontinuous, while the split-step correction produces a much better image. The quality of the image produced with the 16m dual-algorithm (Figure 3) is quite comparable with that generated by recursive integral SNPS algorithm (Figure 4), which is much slower than the dual algorithm. It took about 3 minutes to migrate a shot gather on a single-CPU Alpha XP1000 workstation when the 16m dual-algorithm is used.

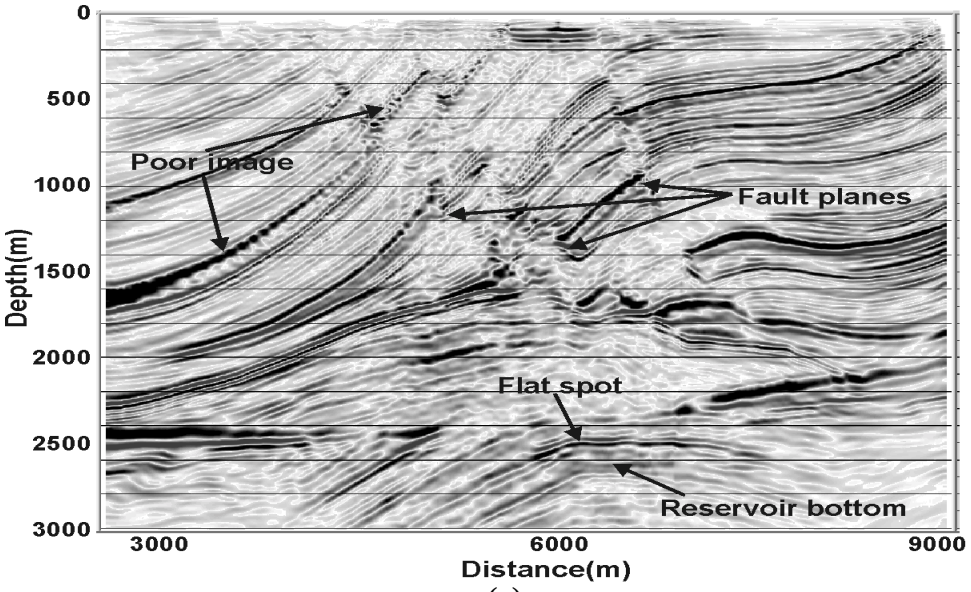

(a)

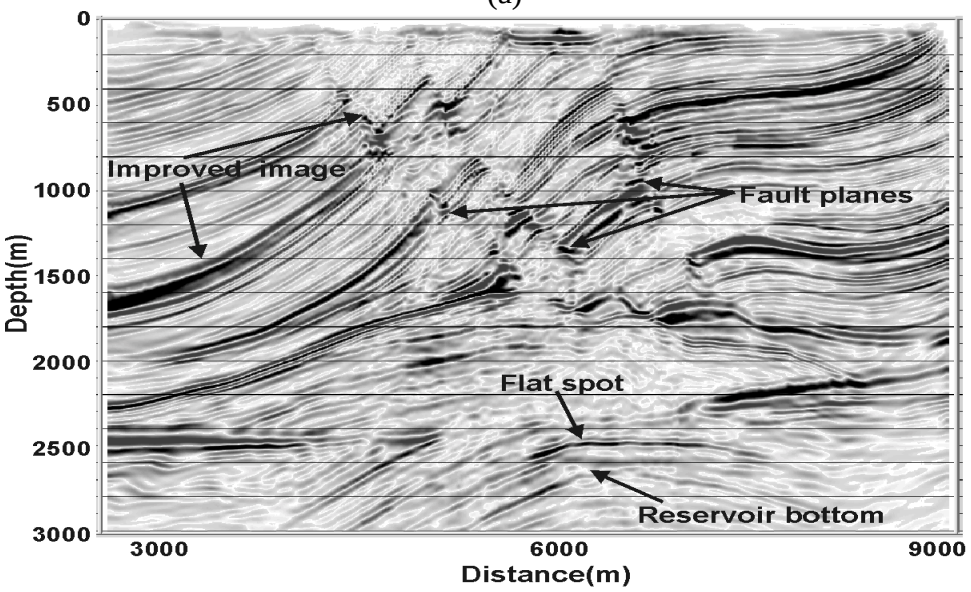

(b)

FIG. 2. Marmousi CIG image computed with a 40-m dual-algorithm by (a) linear interpolation of static phase-shift corrected wavefield and (b) linear interpolation of wavefields corrected with the single-reference-velocity split-step algorithm. Note the phase error generated by the large-step extrapolation on high-dip reflections in (a) and the improvement in (b).

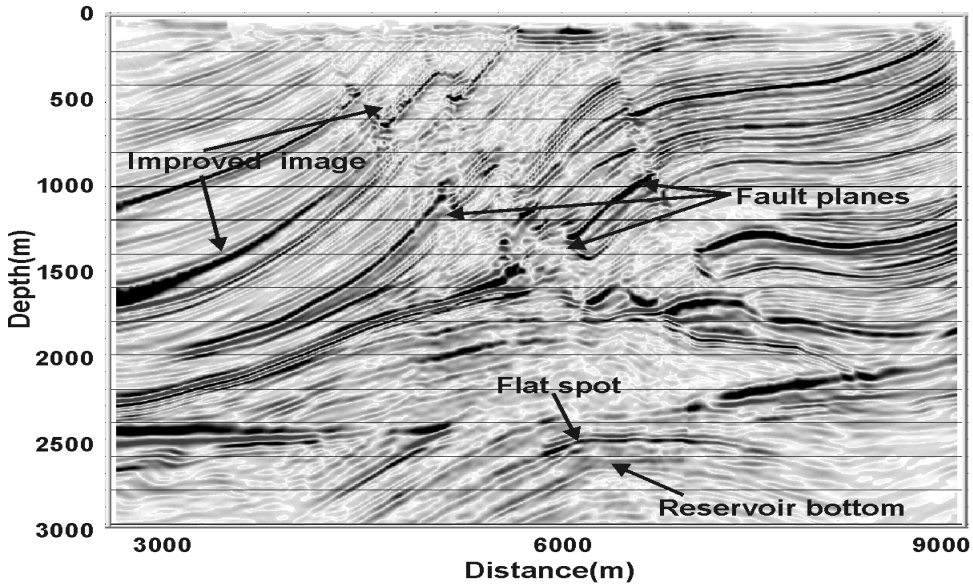

FIG. 3. Marmousi CIG image computed with a 16m dual-algorithm.

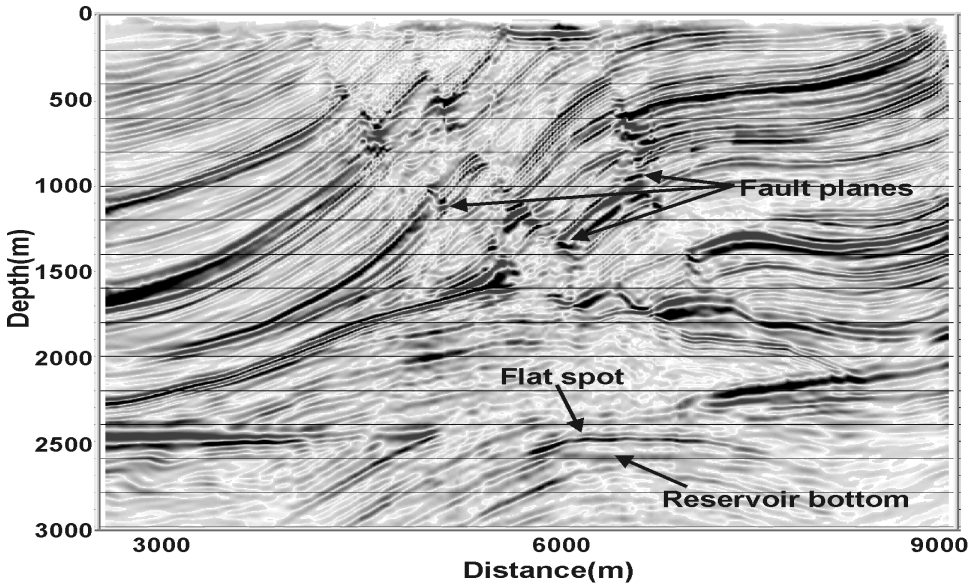

FIG. 4. Marmousi CIG image computed with recursive SNPS integral algorithm.

WAVEFIELD EXTRAPOLATION FROM TOPOGRAPHY WITH LARGE-STEP PSPI AND NSPS

Conventional statics correction is based on the assumption that wave propagates vertically near surface due the presence of low velocity layer. It fails when near-surface velocity is high. Wave equation redatuming that lets waves propagate at all possible angles is required. Figure 5 shows the basic idea of wave equation redatuming. For a complex velocity model, Fourier domain redatuming requires recursive wavefield extrapolation, continuous muting of unnecessary extrapolated wavefield, and inclusion of the wavefield recorded at current depth level until

reaching a flat datum that is typically equal or deeper than the lowest point of the topography.

For less complex media and relatively small topographic variation, recursive wavefield extrapolation can be approximately replaced by a single-step nonstationary wavefield extrapolation with not only laterally varying velocities, but also laterally varying extrapolation step size (Margrave and Yao, 2000) (Figure 6). For example, a PSPI nonstationary redatuming algorithm can be formulated as,

$$\psi(\mathrm{x},z,\omega)=\frac{1}{2\pi}\int_{-\infty}^{+\infty}\alpha(\mathrm{x},\mathrm{k}_\mathrm{x},z,\omega)\varphi(\mathrm{k}_\mathrm{x},0,\omega)\exp(-i\mathrm{k}_\mathrm{x}x)d\mathrm{k}_\mathrm{x}, \tag{23}$$

with the nonstationary wavefield extrapolator $\alpha(\mathrm{x},\mathrm{k}_\mathrm{x},z,\omega)$ written as

$$\alpha(\mathrm{x},\mathrm{k}_\mathrm{x},z,\omega)=e^{\pm ih(x)\sqrt{\frac{\omega^2}{v_{ave}(x)}-k_x^2}}. \tag{24}$$

Note both the velocity and the extrapolation step size are now *x*-dependent. Plus and minus signs denote backward and forward extrapolation.

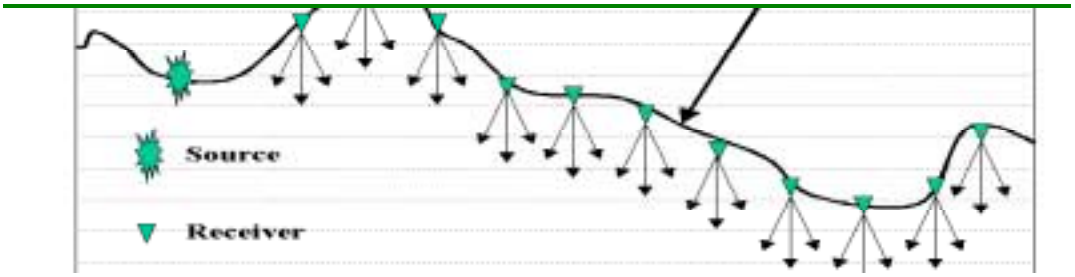

FIG. 5. Wave equation redatuming allows the energy at each receiver location to propagate along non-vertical ray-paths. Grey grid lines are depth steps.

Equation (23) is a large-step algorithm, however different from that previously discussed. Average velocity is used for both static phase-shift and the focusing phase-shift terms. According to the large-step extrapolation algorithm defined before, equation (24) can be split into a static phase-shift and a focusing phase-shift term. The extrapolation can then be written as

$$\psi(\mathrm{x},z,\omega)=e^{-i\Phi(x)_{static}}\left[\frac{1}{2\pi}\int_{-\infty}^{+\infty}\alpha'(\mathrm{x},\mathrm{k}_\mathrm{x},z,\omega)\varphi(\mathrm{k}_\mathrm{x},z,\omega)\exp(-i\mathrm{k}_\mathrm{x}x)d\mathrm{k}_\mathrm{x}\right], \tag{25}$$

where Φ_{static} is the static phase-shift defined as

$$\Phi_{static}=\frac{\omega h(x)}{v_{ave}}. \tag{26}$$

The nonstationary focusing phase-shift operator can be written as

$$\alpha'_{mean}\left(\mathrm{x},\mathrm{k}_\mathrm{x},z,\omega\right)=e^{-i\frac{\omega h(x)}{v_{mean}(x)}\left(\sqrt{1-\frac{k_x^2 v_{mean}(x)^2}{\omega^2}}-1\right)}, \tag{27}$$

where both the average and the mean velocities are computed from the topographic function to a flat datum. Note only the forward extrapolation is considered.

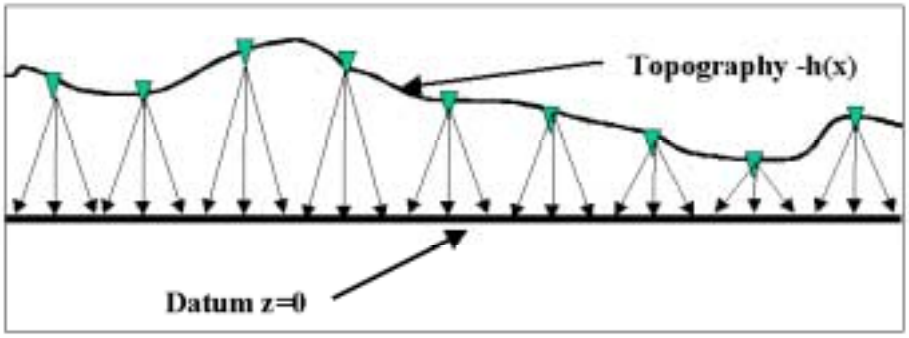

FIG. 6. Single-step Fourier domain redatuming with nonstationary wavefield extrapolator. Both the extrapolation step size and the velocity are functions of spatial location.

For more severe topographic variation and stronger lateral-velocity gradient, an accurate large-angle propagator is desired. Equation (25) can be applied recursively with the *x*-dependent depth step function being a slice of the overall topography z*(x)* in each step; however, a spatial mute function must be applied to eliminate the extrapolated wavefield where the topography is below the extrapolation depth. Data recorded at current depth step is then included for the next step extrapolation. For a large-step PSPI implementation, the thinner the slice is, the more accurate the algorithm is. For a PSPI implementation, each step of extrapolation can be written as,

$$\begin{aligned}\psi\left(\mathrm{x},z_0+\Delta z,\omega\right)=PSPI\left[\varphi\left(\mathrm{k}_\mathrm{x},z_0,\omega\right)\right]W(x,z_0)\\ +\psi_{z(x)}\left(\mathrm{x},z_0\le z<z_0+\Delta z,\omega\right),\end{aligned} \tag{28}$$

where PSPI denote the PSPI integral algorithm. $\varphi\left(\mathrm{k}_\mathrm{x},z_0,\omega\right)$ and $\psi\left(\mathrm{x},z_0+\Delta z,\omega\right)$ denotes the (ω,k_x) domain wavefield at depth z_0 and the (ω,x) domain wavefield at depth $z_0+\Delta z$, respectively. *W(x,z₀)* denotes the spatial windowing function, which is defined as

$$W=\begin{cases}1 & z_0>h(x)\\ 0 & z_0\le h(x)\end{cases}. \tag{29}$$

$\psi_{z(x)}$ denotes the wavefield recorded on the topography *z(x)*. The extrapolation depth-step function in the nonstationary phase-shift operator is now defined as

$$h(x) = h_2(x) - h_1(x) \quad , \tag{30}$$

where $h_1(x)$ and $h_2(x)$ are the x dependent depths functions at z_0 and $z_0 + \Delta z$, defined as

$$\begin{aligned} h_1(x) &= \max\left(z(x), z_0\right) \\ h_2(x) &= \max\left(z(x), z_0 + \Delta z\right), \end{aligned} \tag{31}$$

and $z(x)$ is now the topography.

Figure 7 shows a zero-offset forward extrapolation of 11 impulses through a complex velocity model. The impulses are placed uniformly at the bottom of the model and receivers are placed at each x-location on the topography. Forward modelling is done by recursive application of the PSPI integral extrapolator with a step size of 4 m. The velocity model has a maximum of 100% lateral velocity variation and roughly 110m topographic relief within a 750m distance. Comparison of the downward extrapolation with large-step PSPI extrapolation algorithm with the recursive PSPI integral algorithm shows how robust the large-step algorithm is. Figure 8 shows the inverse extrapolation with the recursive 4m step PSPI integral and large-step algorithm with various step sizes. Note that the quality of the focal points only degrades slightly when the step size is increased to 80m.

The NSPS counterparts of equation (23) can be written as

$$\varphi\left(\mathrm{k_x}, z, \omega\right) = \int_{-\infty}^{+\infty} \alpha\left(\mathrm{x}, \mathrm{k_x}, z, \omega\right) \psi\left(\mathrm{x}, 0, \omega\right) \exp\left(i \mathrm{k_x} x\right) d\mathrm{x} \quad , \tag{32}$$

with the nonstationary wavefield extrapolator $\alpha\left(\mathrm{x}, \mathrm{k_x}, z, \omega\right)$ expressed in equation (24). Similarly, the NSPS counterpart of equation (25) can be written as,

$$\varphi\left(\mathrm{k_x}, z, \omega\right) = \int_{-\infty}^{+\infty} \alpha'\left(\mathrm{x}, \mathrm{k_x}, z, \omega\right) \psi\left(\mathrm{x}, z, \omega\right) \exp(-i\Phi(x)_{static}) \exp\left(i \mathrm{k_x} x\right) d\mathrm{x} \quad , \tag{33}$$

where Φ_{static} is the static phase shift defined the same as equation (26) and the focusing phase-shift $\alpha'\left(\mathrm{x}, \mathrm{k_x}, z, \omega\right)$ is defined the same as equation (27). For multi-step extrapolation through topography, the extrapolated process involves similar muting of the extrapolated wavefield above topography and addition of recorded data at proper depth level.

The spatial Fourier transform requires the seismic data be recorded on a flat datum. Both of equations (23) and (25) requires that the wavefield recorded on a non-flat datum be transformed from x coordinate to k_x coordinate before they can be applied. PSPI extrapolation from topography obviously violates this assumption. The same problem exists for equation (28) since a simultaneous inverse transform has the same assumption. Equation (33) has an advantage that the wavefield is first vertically shifted to a flat datum with an average interval velocity, which is equivalent to a statics correction and then extrapolated and forward transformed to the k_x domain.

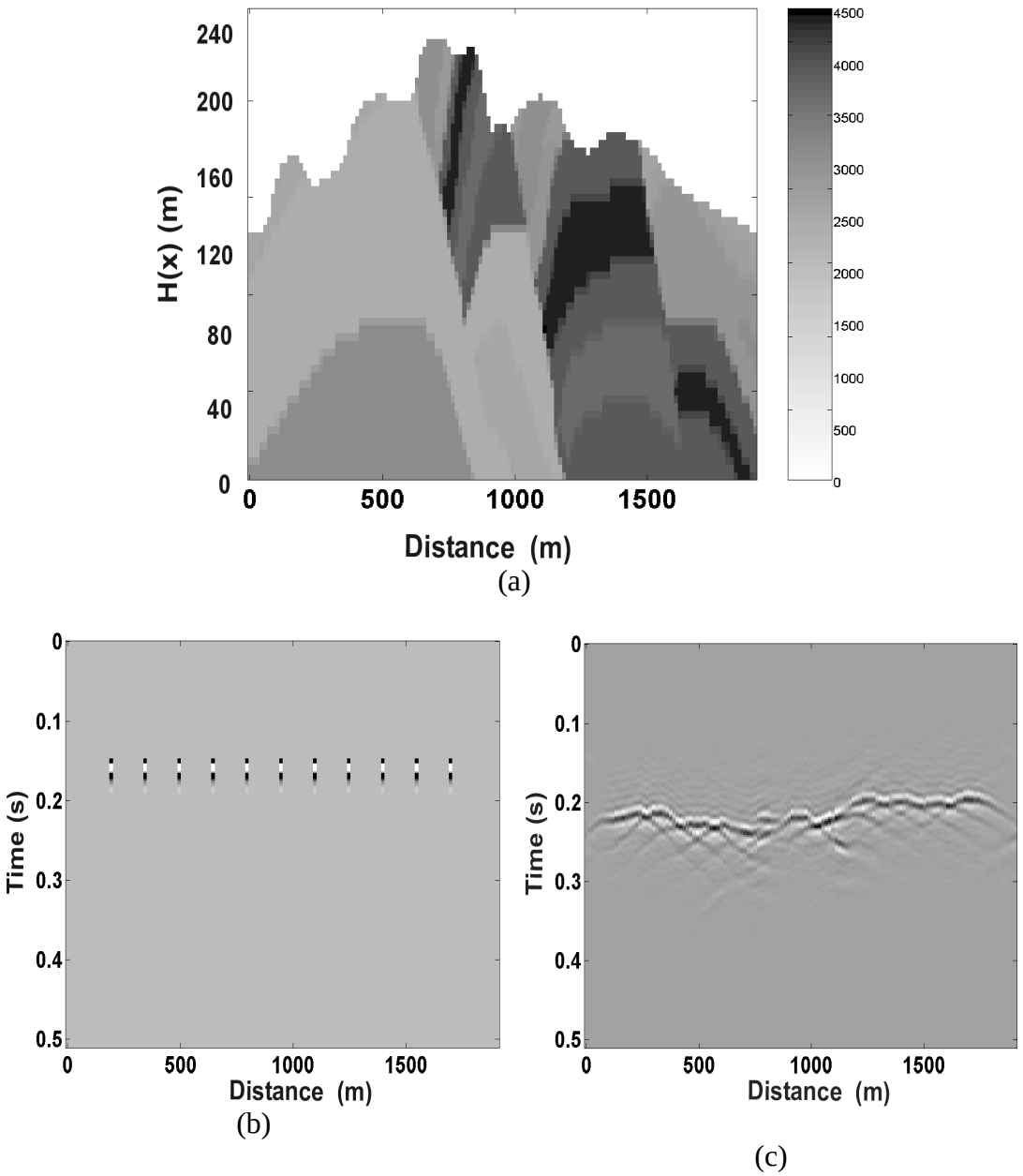

FIG. 7. Zero-offset forward extrapolation with recursive PSPI integral of 4-m step size. (a) The velocity model, (b) the 11 impulses, (c) the zero-offset synthetic.

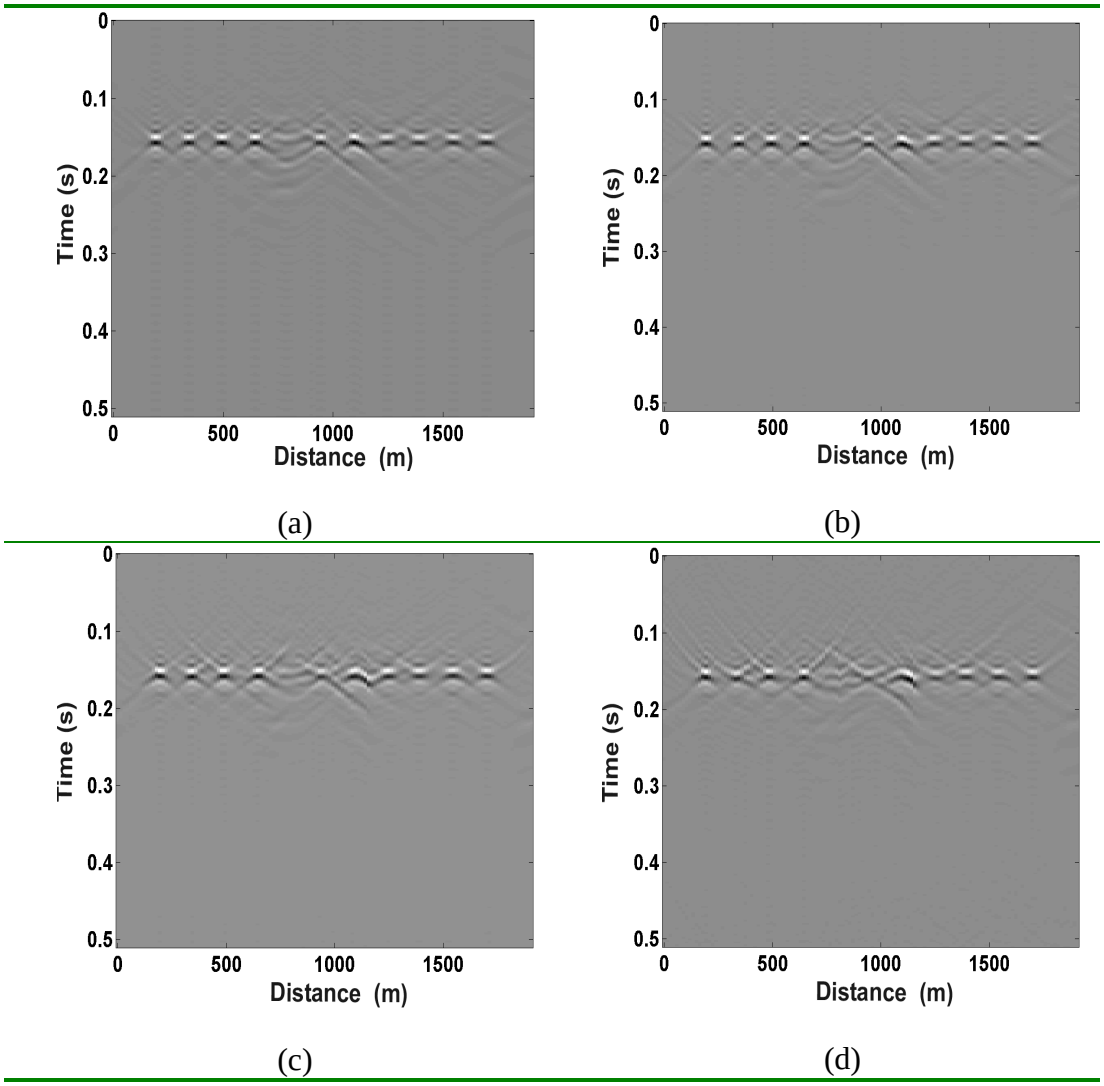

FIG. 8. Accuracy comparison of inverse extrapolation. (a) Recursive PSPI integral extrapolator with 4m step size, (b) inverse extrapolation with 20m PSPI integral extrapolator, (c) inverse extrapolation with 80m PSPI integral extrapolator, (d) inverse extrapolation with 120m integral extrapolator.

Figure 9 shows NSPS forward and inverse extrapolation test similar to that shown in Figure 8. The difference between the modelled data with PSPI integral and the NSPS integral is minor, however the energy of the events around x=750m, corresponding to the highest point of the topography and greatest lateral velocity contrast, is more complete and stronger. Figure 9b-d shows large-step inverse extrapolation of Figure 9a with 80m, 120m and 160m NSPS integral extrapolation. The source impulse at x=750m is missing in the PSPI extrapolation test due to severe topographic variation and high lateral velocity contrast. However NSPS is able to recover the source impulse very well even when the extrapolation step size is increased to 160m.

For depth imaging, the wavefield at each depth-step within the topography can be computed by either recursive extrapolation or the dual algorithm, with the spatial muting function W applied and field data recorded at current depth level added.

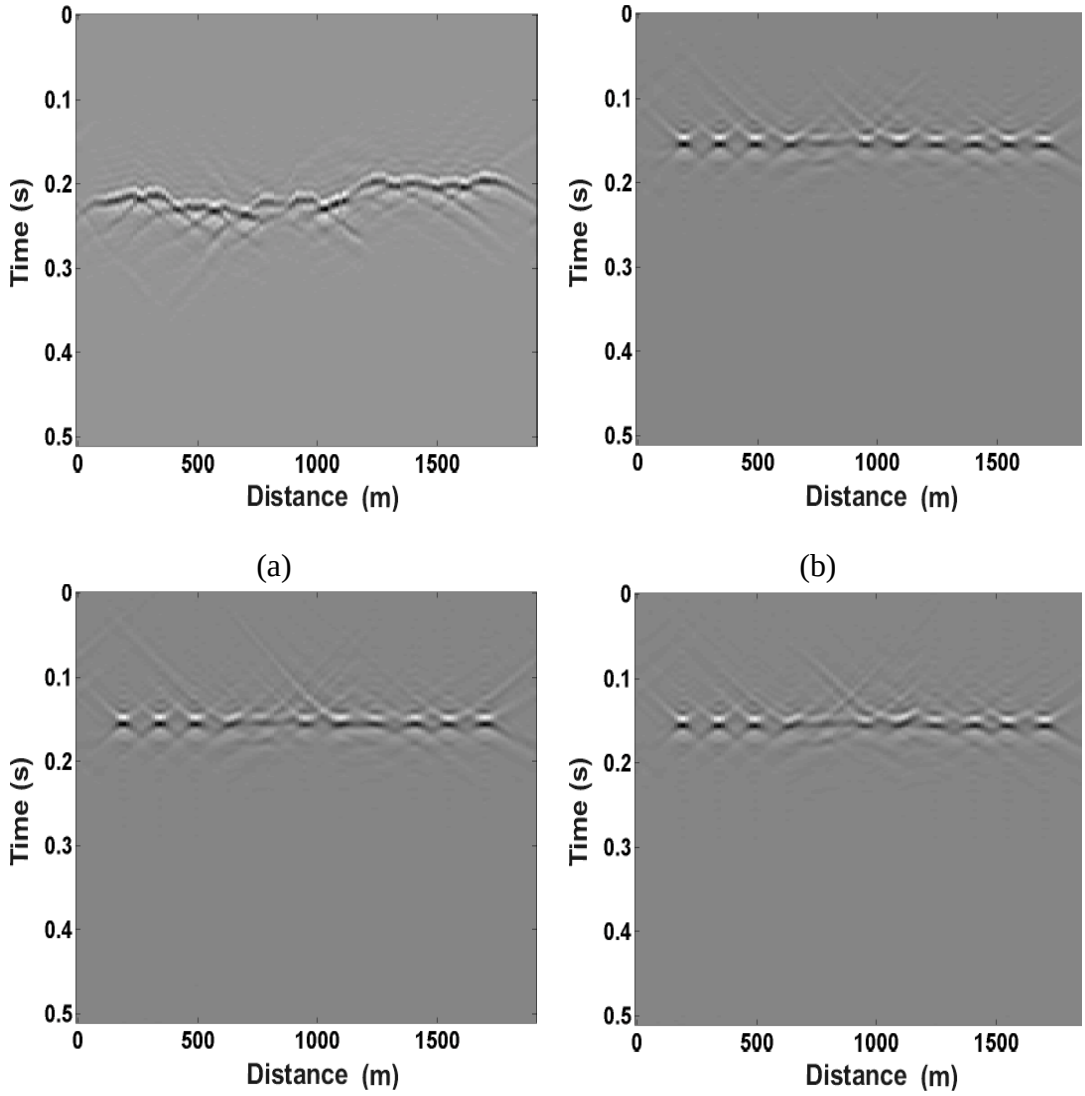

FIG. 9. Zero-offset extrapolation test with large-step NSPS. (a) Recursive NSPS with 4m step size, (b) inverse extrapolation with a 80m NSPS, (c) inverse extrapolation with a 120m NSPS and (d) inverse extrapolation with a 160m NSPS.

APPLICATION OF PSPI DUAL-ALGORITHM TO THE FOOTHILLS SYNTHETIC DATA SET

We now show results from a finite-difference synthetic 2-D seismic line that models the extreme topography and velocity variation of the Canadian Rocky Mountains. This model was provided by Sam Gray (then of AMOCO) (Gray and Marfurt, 1995) and thanks are also due to BP for allowing its use. Figure 10 shows a geologic cross-section representative of northeastern British Columbia, where large topography variation and high-angle thrust faults are common. The model contains a

number of faults and folded layers, as well as roughly 1600m of elevation relief that is typical in Canadian Rocky regions. The model is 25km long. The highest topography is about 2km above sea level and the deepest part is about 8km below sea level. The model has P wave velocity variation from 3600m/s near the surface and 5900m/s near the bottom. The depth model sample rate is 10m. A total of 278 2-D synthetic shot gathers were computed with finite-difference modelling. The data were recorded to 5s by a split spread of 480 receivers with offsets ranging from 15m to 3600m on both sides of the shot points. The shot spacing was 90m and the original time sample rate is 4ms. The 2-D cylindrical spreading loss is proportional to $t^{-1/2}$. A geometrical spreading correction should be applied before imaging.

The dominant frequency content of the original synthetic data is from 5Hz to 40Hz. It allows resampling to 6ms rate to reduce the amount of computation. Each shot gather was padded to 7.5s to accommodate the energy wrapped around by the extrapolation and Fourier transform, which becomes noise when it is not handled properly. A more efficient approach is to only pad small amount of time to the traces and mute the padded region after each large-step extrapolation or after several steps of extrapolation, as long as the vertical traveltime shift in the extrapolation does not exceed the padded time. Each shot gather was padded to 512 traces with the source located in the middle, so that there are 15 padded traces (225m) on both sides to accommodate the energy wrapped around by extrapolation and spatial Fourier transforms. The padded traces are muted after each large-step extrapolation. For a step size of 50m, the padding can handle a design dip of 78 degrees. This is often good enough for most complex geology settings.

Figure 11 shows a shot gather located in the middle of the model. Rapid topography variation, high near-surface velocity and complex structures present a great challenge to depth imaging algorithms.

A PSPI dual-algorithm was implemented on the MACI cluster workstations. A total of 14 computing nodes were used and it took about 8 hours to migrate all the whole data set. Figure 12 shows the shot gather in Figure 11 after migration and Figure 13 shows a CIG at the middle of the line. Figure 14 show a) the CIG stack and two images produced by other authors, b) a prestack Kirchhoff migration (Gray and Marfurt, 1995) and c) a 75-degree finite-difference prestack migration by H. Lu in the CREWES Project with the prestack finite-difference depth migration module in ProMAX. The result produced by the large-step PSPI integral algorithm has several advantages over other algorithms, not only in term of the near-surface events, but also in term of migration noise level and vertical image resolution. The Kirchhoff algorithm fails to recover both of the flanks of the syncline that is located in the middle of model and at depth from 7000m to 8000m. The major near-surface events are clear, however the migration noise is very disturbing. Figure 15 shows a zoomed version of the upper-left corner of the images Figure 14. Improvement is obvious. The 75-degree finite-difference algorithm produced a less noisy image, however the image depth is slightly incorrect. This is apparent that the left end of the basement reflection should be at 10000m instead of 10300m. The quality of the dominant fault plane on the right of the section, as well as the strata on both sides, tells the algorithms' capability in imaging high-dip events. Apparently the large-step PSPI integral algorithm produced the best result.

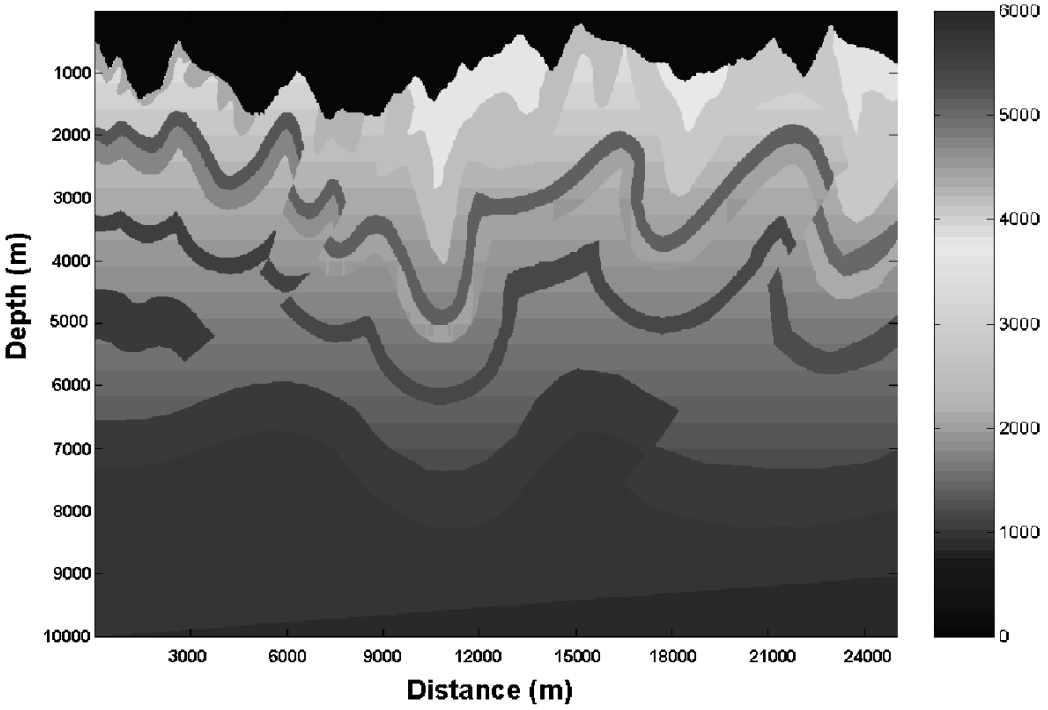

FIG. 10. A velocity/depth model representative of northeastern British Columbia (after Gray and Marfurt, 1995).

COMPARISON OF SPEED AND LIMITATIONS OF WAVEFIELD EXTRAPOLATION ALGORITHMS

The NSP, PSPI and SNPS are $N_sN_zN^3$ algorithms. The order of other Fourier-domain prestack-depth-imaging methods can be computed in a similar way. For a single-reference velocity, split-step Fourier methods (or phase-screen method), ignoring the computation time for vertical travel time correction since computing the focusing term consume the most computer time, the computational cost function can be written as $N_sN_zN^2logN$. For a windowed split-step approach, the computer time cost function can therefore be written as $N_sN_zN_wN^2logN$, where N_w is the number of lateral windows. Gazdag's PSPI approach roughly is of the same order as a windowed split-step Fourier method. Its computing cost function can be written as $N_sN_zN_vN^2logN$, where N_v is the number of reference velocities. For the dual algorithm, the cost function can be written as $N_sN_zN^3/N_L$, where N_L is the number of intermediate steps in a large-step extrapolation. When the condition $N_vlogN > N/N_L$ is satisfied, the dual algorithm becomes faster than the windowed split-step Fourier method and Gazdag's PSPI approach. Table 1 shows the relative performance of different Fourier domain wavefield extrapolators. This is only a rough estimation and can only be viewed in a relative sense.

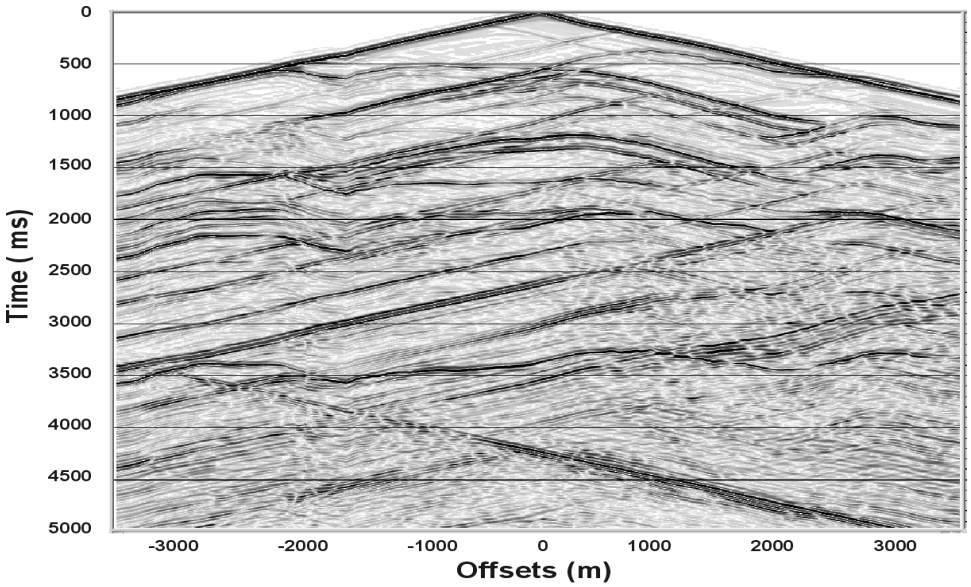

FIG. 11. A shot gather located in the middle of the model.

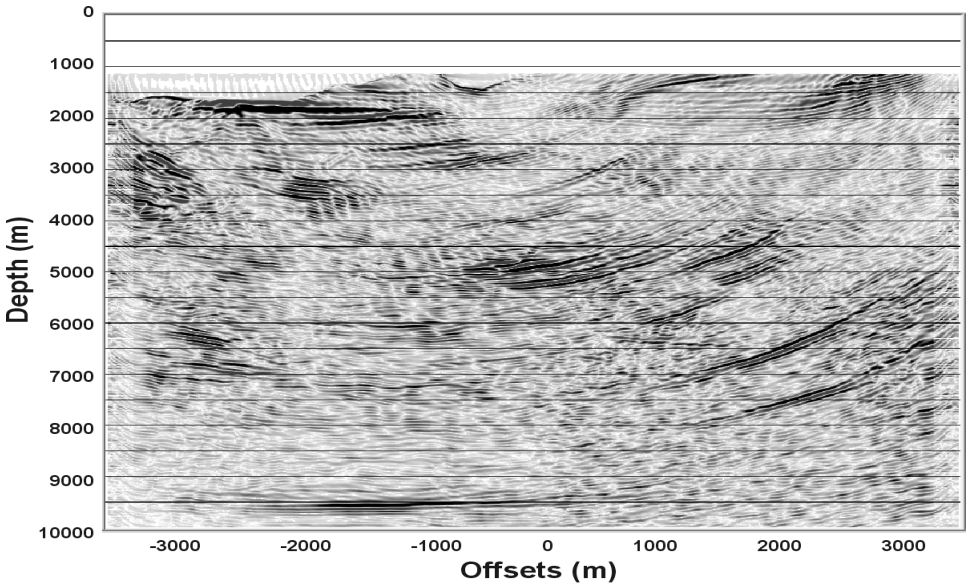

FIG. 12. Shot gather of Figure 11 after migration from topography with the dual algorithm. The extrapolation step is 50m.

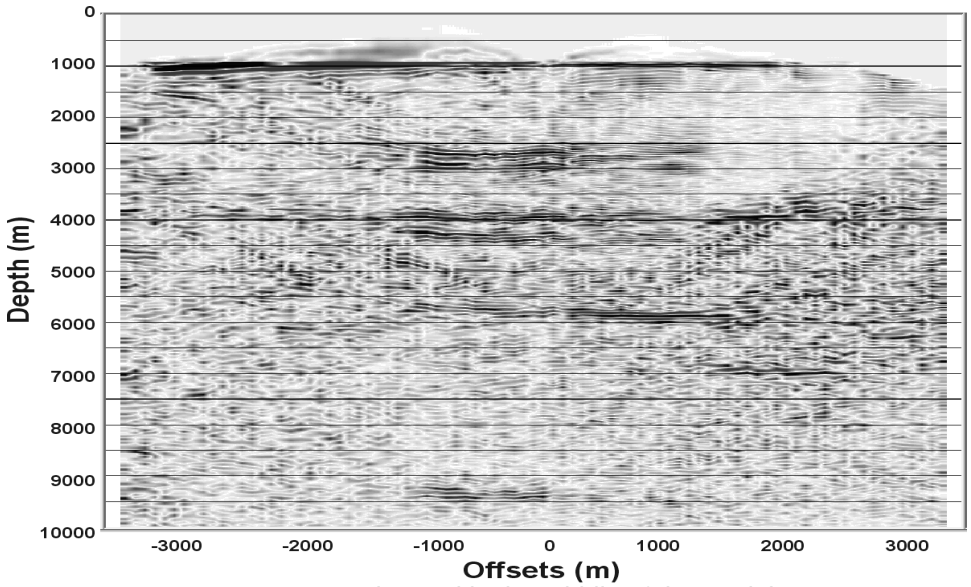

FIG. 13. A CIG located in the middle of the model.

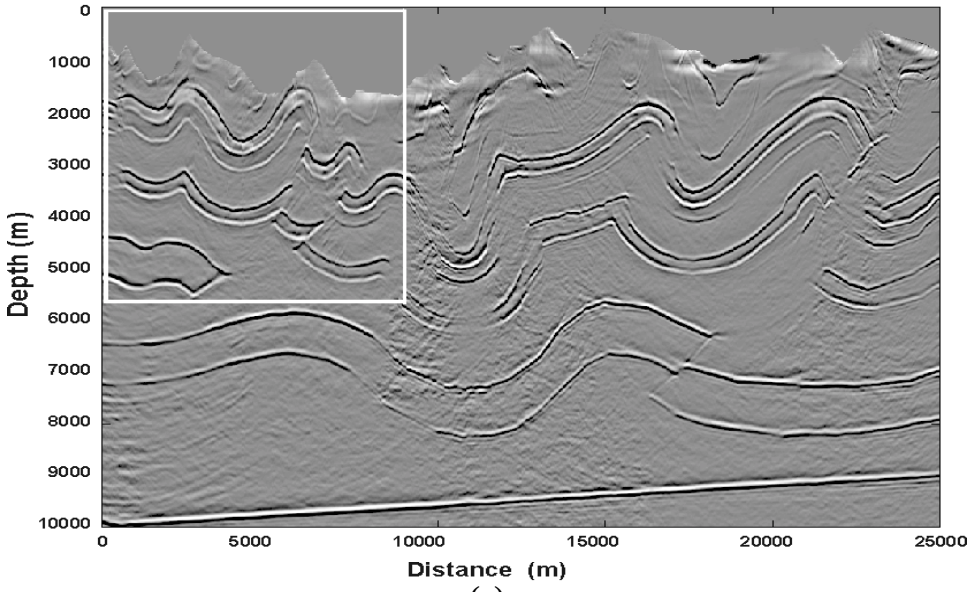

(a)

FIG. 14. (Text overleaf)

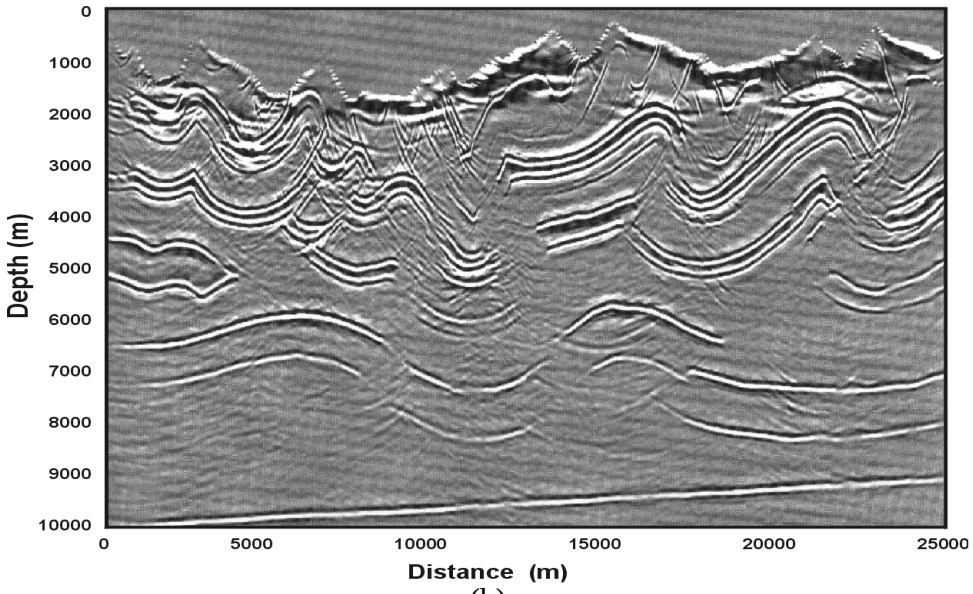

(b)

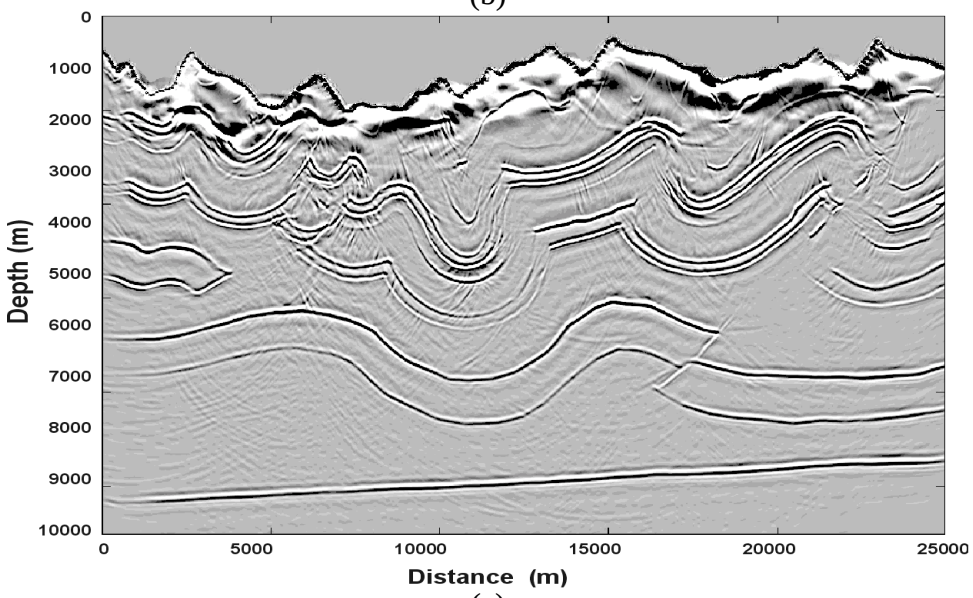

(c)

FIG. 14. (a)The depth image computed with the PSPI dual algorithm; (b) the depth image computed with Kirchhoff migration from topography and (c) the depth image computed with 75-degree finite-difference algorithm.

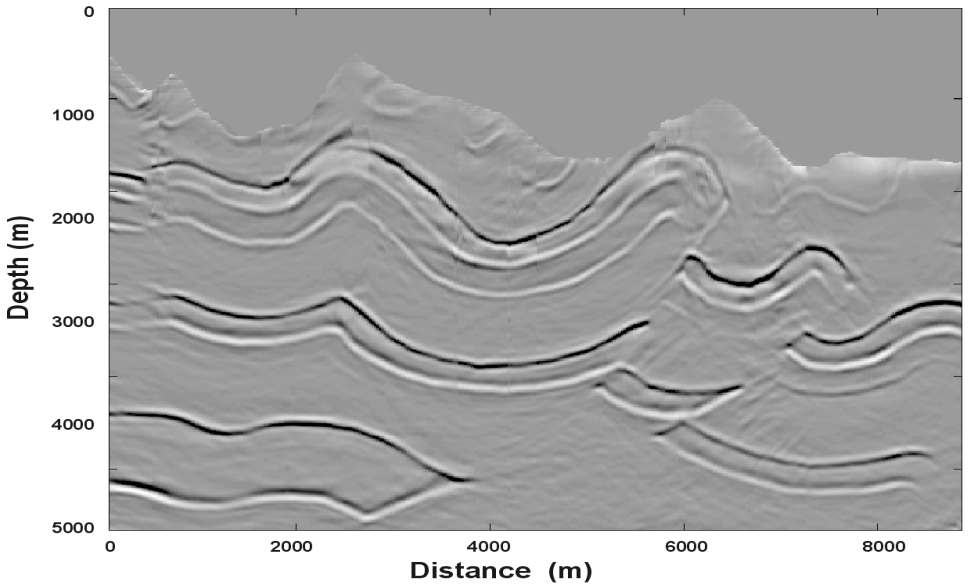

(a)

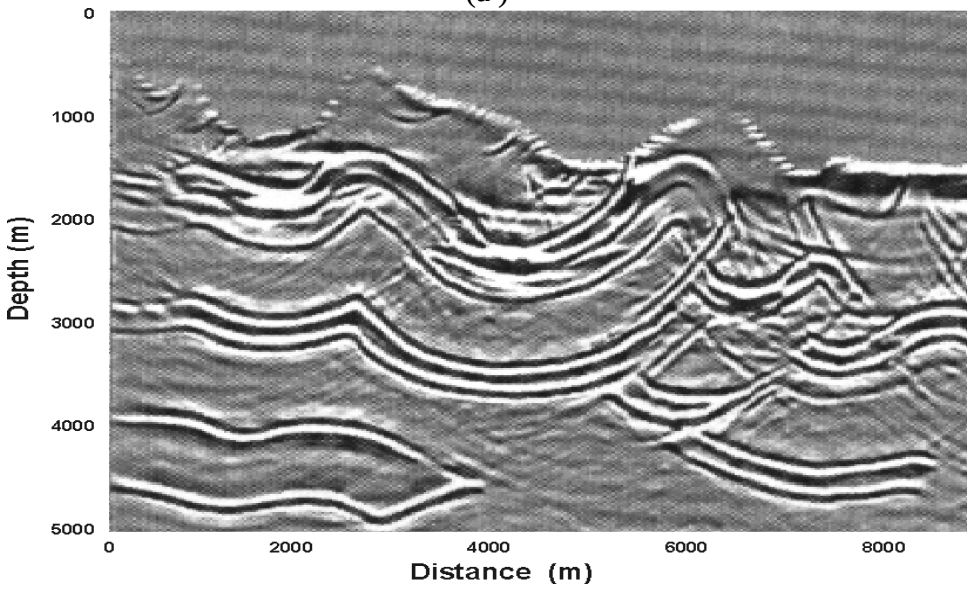

(b)

FIG. 15. (Text overleaf)

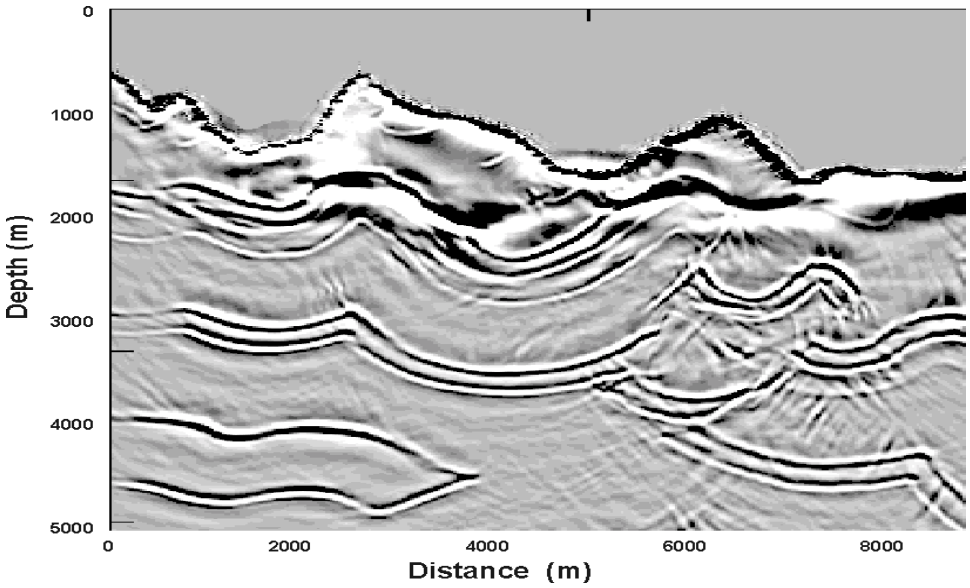

(c)

FIG. 15. Zoom of the upper-left portions of the images in Figure 14. (a) Zoom of Figure 14a; (b) Zoom of Figure 14b; (c) zoom of Figure 14c; (d) zoom of Figure 14d.

Algorithms	Ability to Handle Large Lateral Velocity Gradient	Order of Algorithm	Relative Speed
NSPS, PSPI and SNPS Integrals	Strong	$N_s N_z N^3$	Slow.
Dual Algorithm	Strong	$N_s N_z N^3 / N_L$	Very fast.
Split-step / Phase-screen	Weak	$N_s N_z N^2 \log N$	Very fast.
Windowed Split-step / Phase-screen	Strong when sufficient numbers of windows are used.	$N_s N_z N_w N^2 \log N$	Slow when the number of windows exceeds N/logN.
Gazdag's PSPI	Strong when sufficient number of reference velocities is used.	$N_s N_z N_v N^2 \log N$	Slow when number of reference velocities exceeds N/logN.

Table 1. Performance summary of established Fourier domain imaging techniques.

CONCLUSIONS

The large-step nonstationary integral wavefield extrapolators prove to be accurate and effective for prestack depth imaging. It dramatically reduced the run-time of the nonstationary integral wavefield extrapolators and suitable for regions of complex geology. This is demonstrated by applying the PSPI dual-algorithm to the Marmousi synthetic dataset. The dual-algorithms are also very adaptive to regions of large topographic variation superimposed with high surface velocity and high velocity contrast. This is demonstrated with prestack depth migration of the Foothills synthetic data and comparison with images produced by previous authors.

ACKNOWLEDGEMENTS

We thank Sam Gray and BP for the topographic synthetic dataset and Han-xing Lu for her processing of it. Zhengsheng Yao provided helpful consultation. We are grateful for the financial support of the sponsors of CREWES.

REFERENCES

Gazdag, J. and Sguazzero, P., 1984, Migration of seismic data by phase-shift plus interpolation, Geophysics, 49, 124-131.

Gray, S.H. and Marfurt, K.J., 1995, Migration from topography: Improving the near-surface image: J. Can. Soc. Expl. Geophys., **31,** no. 1/2, 18-24.

Margrave, G.F. and Yao, Z., 2000, Downward extrapolation from topography with a laterally variable depth step, 70th Ann. Internat. Mtg: Soc. of Expl. Geophys., Session: IMG 2.1.

Mi, Y. and Margrave, G.F., 2000, Dual extrapolation algorithms towards optimum efficiency and accuracy, CREWES Research Report, Vol. 12.

Ng, M., 1994, Prestack migration of shot records using phase-shift plus interpolation: J. Can. Soc. Expl. Geophys., 30, no. 01, 11-27.